# Neutron Emission from Compound Nuclear Systems of High Angular Momentum*

H. W. Broek†
*Yale University, New Haven, Connecticut, and Argonne National Laboratory, Argonne, Illinois*
(Received May 26, 1961)

Measurements were made of the energy spectra and angular distributions of neutrons emitted with laboratory energies in the range from 1 to 10 Mev in reactions induced by 160-Mev oxygen-16 ions incident on thin targets of aluminum, nickel, copper, and gold. Spectra were obtained (at laboratory angles between 30° and 150°) by analysis of the proton-recoil pulse-height spectra produced by the neutrons in a stilbene scintillation crystal. All spectra and angular distributions at these angles are consistent with the hypothesis of evaporation from compound nuclei. The energy spectra of neutrons emitted from the initial compound nuclei were calculated by use of statistical evaporation theory, both with and without modification to include (in a classical approximation) the effects of conservation of angular momentum. The dominant effect of conservation of angular momentum upon the calculated neutron spectra from the initial compound nuclei is a lowering of the nuclear emission temperature for the cases and parameters chosen. The measured spectra are compared to the spectra calculated both with and without the modification. The angular distributions are symmetric about 90° and peaked forward and backward. The total cross section for neutron production increases with increasing mass of the target atom, and is roughly 70% greater for copper than for nickel. This sudden increase is probably related to the greater neutron excess of copper.

## I. INTRODUCTION

THE evaporation of particles from an excited nucleus was first treated mathematically by Weisskopf[1] who based his work on the compound-nucleus assumptions of Bohr.[2] The theory contains the level-density function which depends upon excitation energy, angular momentum, and other details of nuclear structure. The theory predicts that the emitted neutrons will have an approximately Maxwellian distribution, that the energy distribution of emitted charged particles will have a peak near the Coulomb barrier, and that the angular distributions will be symmetric about 90° if the levels have random phases.[3] Some experiments confirm these predictions.[4] However, experiments on inelastic scattering show too many high-energy emitted particles,[5] the residual nucleus is left in a low-lying excited state more often than is expected from the statistical theory, and the angular distributions are strongly peaked forward. Explanation of these results requires direct or surface interaction models, in which no compound nucleus is formed.[6] Nevertheless, the energy spectra of the lower-energy emitted particles are consistent with evaporation theory.

A complication in experimental work at higher energies is that the incident proton or alpha particle often does not deposit its full energy in the target nucleus. Hence a distribution of initial excitation energies exists even for monoenergetic incident particles, and makes interpretation of results more difficult.[7]

An alternative way of producing highly excited states of the compound nucleus is afforded by heavy-ion reactions.[8] In these reactions, several nucleons are simultaneously incident at lower energy per nucleon. The compound system is likely to have the maximum initial excitation energy that the heavy ion can deposit. Also the heavy ion imparts a greater angular momentum to the compound system than does a proton or alpha particle of the same energy, and thus compound states of high angular momentum can be produced.

Evaporation of charged particles from reactions induced by bombarding nickel with oxygen ions having an energy of 10 Mev per nucleon was studied by Knox *et al.*[9,10] who found that the most frequently emitted charged particles are protons and alpha particles. Energy spectra peak below the barrier energy and below the theoretical peak energy calculated on the basis of statistical theory by Dostrovsky *et al.*[11] This effect may be due to barrier lowering at high excitation. The part of the nuclear potential that is produced by excited nucleons may appear more at the nuclear edge and may make the edge become progressively more diffuse with increasing excitation. This effect, which has been studied by Fulmer and Goodman[12] for $(\alpha,p)$ reactions, could be included in evaporation calculations since the reverse cross section which they employ is that for the emitted particle incident on the excited residual nucleus and not on the ground state of the residual nucleus. Evaporation calculations so far have not treated this distinction adequately. The spectra of particles emitted from reactions induced by heavy ions are also affected by the dependence of level density

* Work performed under the auspices of the U. S. Atomic Energy Commission.
† Now at Argonne National Laboratory, Argonne, Illinois.
[1] V. F. Weisskopf, Phys. Rev. **52**, 295 (1937).
[2] N. Bohr, Nature **137**, 344 (1936).
[3] H. A. Bethe, Revs. Modern Phys. **9**, 69 (1937).
[4] P. C. Gugelot, Phys. Rev. **81**, 51 (1951); E. R. Graves and L. Rosen, *ibid.* **89**, 343 (1953).
[5] P. C. Gugelot, Phys. Rev. **93**, 425 (1954); R. M. Eisberg, *ibid.* **94**, 739 (1954); R. M. Eisberg and G. Igo, *ibid.* **93**, 1039 (1954).
[6] N. Austern, S. T. Butler, and H. McManus, Phys. Rev. **92**, 350 (1953); S. T. Butler, *Nuclear Stripping Reactions* (John Wiley & Sons, Inc., New York, 1957).
[7] R. Serber, Phys. Rev. **72**, 1114 (1947).
[8] J. H. Fremlin, in *Nuclear Reactions*, edited by P. M. Endt and M. Demeur (North-Holland Publishing Co., Amsterdam, 1959), Vol. I, p. 86.
[9] W. J. Knox, A. R. Quinton, and C. E. Anderson, Phys. Rev. Letters **2**, 402 (1959).
[10] W. J. Knox, A. R. Quinton, and C. E. Anderson, Phys. Rev. **120**, 2120 (1960).
[11] The method of calculation is described by I. Dostrovsky, Z. Fraenkel, and G. Friedlander, Phys. Rev. **116**, 683 (1959).
[12] C. B. Fulmer and C. D. Goodman, Phys. Rev. **117**, 1339 (1960).

upon angular momentum, a dependence which the evaporation calculations usually do not include.

The angular distributions found by Knox *et al.*[9,10] for protons and alpha particles from nickel bombarded with oxygen are nearly symmetric about 90° in the center-of-mass system. This distribution is explained by an evaporation mechanism for most of the particles and a direct or surface interaction for any excess of particles in the forward direction. The fact that the distribution is peaked both forward and backward indicates a tendency for particles to be emitted from the equator of the spinning compound system.

While no previous data on neutron energy spectra and neutron angular distributions from heavy-ion reactions are known, the total neutron production from heavy-ion reactions was measured by Hubbard *et al.*[13] by use of carbon, nitrogen, and neon beams with several targets. These investigators found that the cross section for neutron production increases with increasing atomic number of the beam particle for constant beam velocity. This effect is probably primarily due to increasing excitation energy. The cross section for neutron production also increases with the atomic number of the target particle since charged-particle emission becomes progressively less likely owing to the increasing Coulomb barrier. The cross section for neutron production varies roughly linearly with beam energy.

To further the study of heavy-ion evaporation reactions, neutron energy spectra and angular distributions were measured by use of targets of aluminum, nickel, copper, and gold and a beam of 160-Mev oxygen ions produced by the Yale heavy-ion linear accelerator. Calculations of the energy spectra of particles emitted from the fully excited compound nuclei were made and compared to the experimental energy spectra.

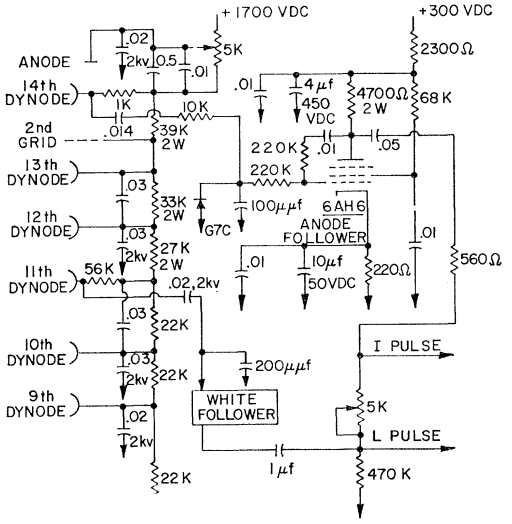


FIG. 1. Diagram of photomultiplier circuit with preamplifiers. Resistors of 22 kilohms are used between all consecutive pairs of dynodes not shown. A 46-kilohm resistor is used between cathode (ground) and the first dynode. The first dynode is connected directly to the first grid. A type 6810-A photomultiplier is used.

[13] E. L. Hubbard, R. M. Main, and R. V. Pyle, Phys. Rev. **118**, 507 (1960).

## II. EXPERIMENTAL METHOD

### A. The Stilbene Scintillation Crystal as a Neutron Spectrometer

The neutron spectra and angular distributions were measured by use of a single stilbene scintillation crystal as a neutron spectrometer, in the manner described by Broek and Anderson.[14] In this spectrometer, the pulse-height spectrum of scintillations produced in a stilbene crystal by recoil protons originating in the crystal is analyzed to yield the energy distribution of the incident neutrons, and pulses due to gamma rays and electrons are rejected by utilizing differences in the pulse shapes of the scintillations produced by electrons and protons.[15]

The measurements were made by use of the techniques described by Broek and Anderson[14] except that the circuit was modified in order to increase the allowable counting rate. In the original discrimination circuit, pulses due to two or more small pulses from electrons detected in near coincidence could add together and produce a spurious gating pulse. This pileup effect limited the allowable counting rate. A new circuit was developed to decrease pileup effects. The basic idea of the new circuit, Fig. 1, is to eliminate the fast component entirely in order to produce an identification pulse that is roughly proportional to the slow component and then by subtraction to compare this pulse to the total pulse. If the slow component is greater than a certain proportion of the total, the pulse is presumed to be due to a proton and the analyzer is gated "on."

As in the previous circuits,[14,15] the voltage from the last dynode to the anode is reduced to allow space-charge saturation to occur. In the new circuit, Fig. 1, charge arriving at the fourteenth (last) dynode is integrated by the interelectrode and stray capacitance and decays (through a 1 K resistor) with a 20-nsec decay time. Because of space-charge saturation, the resulting pulse is negative during and immediately after the fast component (except for the smallest pulses, which do not produce space-charge saturation), but positive during the slow component since the slow component does not saturate the tube. A resistor-diode combination eliminates most of the negative spike caused by the fast component, and the resulting pulse is integrated to obtain a pulse whose height is roughly proportional to the total slow component of scintillation.

[14] H. W. Broek and C. E. Anderson, Rev. Sci. Instr. **31**, 1063 (1960).

[15] R. B. Owen, IRE Trans. Nuclear Sci. **NS-5**, 198 (1958); F. D. Brooks, Nuclear Instr. **4**, 151 (1959).

An anode follower is used to integrate the pulse and invert its polarity. The resulting pulse is then added to the ordinary pulse by means of a resistance network. (The characteristic impedance of the outgoing signal cable is used as one leg of this network.) The resulting pulses are negative for about 2 $\mu$sec for protons and for electrons whose energy is so low that only 2 or 3 photoelectrons arrive at the first dynode of the photomultiplier tube, while electrons of higher energy produce positive pulses in this interval. The pulses are amplified and inverted and fed into a discriminator that allows the largest positive pulses to produce gating pulses which gate the analyzer "on." Pileup of very small pulses due to low-energy electrons cannot produce a gating pulse unless the pulses come within 2 $\mu$sec of each other. The tolerable counting rate was therefore higher than before.

The circuit of Fig. 1 gives two pulses each time a charged particle deposits energy in the crystal. One is the positive $L$ pulse proportional to the total light in the scintillation, and the other is an identification pulse ($I$ pulse) whose negative magnitude is large only for proton-induced scintillations. Both of these pulses are fed from the target area to the experimental area of the laboratory through cables which are terminated in matching resistors at the experimental area.

The $I$ pulse is fed to a Baird-Atomic model 215-m amplifier (Fig. 2) which contains an integral discriminator. The discriminator level is set so that it does not trigger for $I$ pulses due to electrons. This discrimination pulse is then inverted by an anode follower, and fed to the trigger input of the Radiation Instrument Development Laboratories (RIDL) 400-channel analyzer.

The $L$ pulse is passed through a 1-$\mu$sec delay line. This delay compensates for delay in the firing of the discriminator, and greatly reduces the possibility that a count may be missed. The $L$ pulse is fed through a White follower into a simple high-pass resistance-capacitance network with a time constant of 50 $\mu$sec, followed by a low-pass resistance-capacitance network with a time constant of 0.2 $\mu$sec. The shaped pulses are amplified by a TMC model AL-4A amplifier that uses a 1-$\mu$sec delay line to clip the pulses. The pulses are then sent to the analyzer to be analyzed.

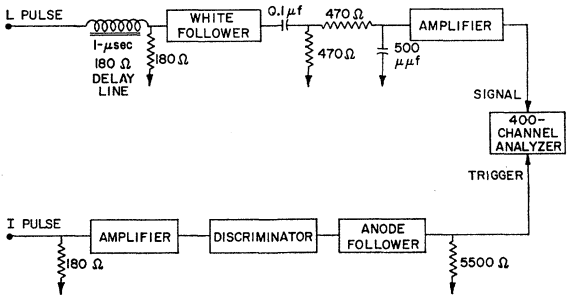


FIG. 2. Arrangement of delaying, amplifying, shaping, and discriminating circuits.

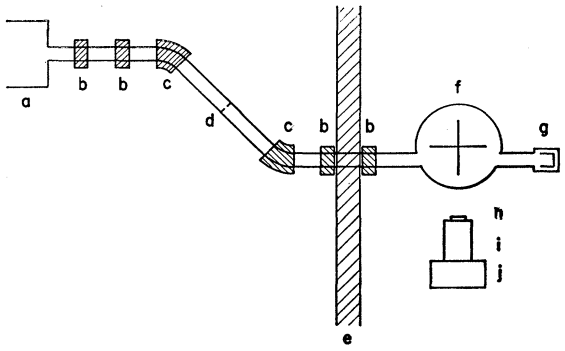


FIG. 3. Schematic diagram of the experimental apparatus. Not to scale. (a) Accelerator tank. (b) Focusing magnet. (c) Analyzing magnet. (d) Energy-defining slit (set to 0.25 in. wide). (e) Concrete shielding wall. (f) Scattering chamber with target holder. (g) Faraday cup. (h) Stilbene crystal. (i) 6810-A photomultiplier. (j) Preamplifiers.

It was necessary to modify the RIDL 400-channel analyzer for this work. Normally the pulse to be analyzed turns on a trigger circuit that actuates the circuits that perform the analysis. The fact that both kinds of pulses can turn this trigger circuit on results in much unnecessary dead time when high counting rates are used in a large gamma-ray background. Therefore the analyzer was modified so that the discrimination pulse from the anode follower turns this trigger on.

The most satisfactory neutron energy calibration available at this accelerator was made by running the $Be^9(\alpha,n)$ reaction at 4 Mev. Three groups of neutrons were observed whose energies were known accurately. A disadvantage is that two to three hours of beam time must be used for calibration. Observations were made at 0°, where the cross sections have large maxima and the variation of neutron energy with angle is small.

Energy calibration can also be accomplished by exposing the crystal to gamma-ray sources, observing the pulse-height spectrum due to the Compton effect, and then using the data of Broek and Anderson[14] to relate electron pulse heights to proton pulse heights. Energy calibration is also possible by use of the Pu-Be neutron source, but the lack of sharp features in the Pu-Be neutron spectrum prevents it from yielding an accurate calibration.

### B. Description of the Scattering Apparatus

A beam of 10.5-Mev/nucleon oxygen ions from the Yale heavy-ion linear accelerator (a in Fig. 3) is passed through a system of focusing magnets $b$ and analyzing magnets $c$, through a target $f$, and into a Faraday cup $g$ where it is integrated. The relatively large distance (1.5 m) from the target to the Faraday cup serves to reduce the background count caused by neutrons produced in the Faraday cup. To reduce background further, the Faraday cup is lined with graphite. Neutron-producing reactions in the Faraday cup are

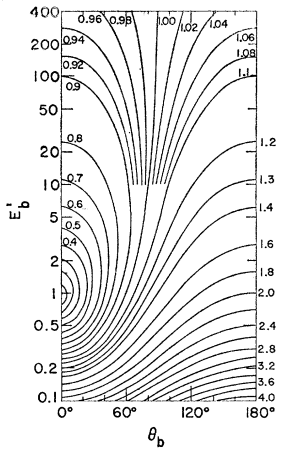


FIG. 4. Transformation factor for the double differential cross section $d^2\sigma/dEd\Omega$ as a function of angle and reduced energy in system $b$.

therefore of the type $O^{16}(C,nx)$. Because of the high velocity of the center of mass in this reaction, most of the neutrons are emitted forward in the laboratory system and have only a minute chance of finding their way back to the detector. Another reason for using carbon is that the total thick-target neutron yield is less from carbon than from materials of higher atomic number.[13] No collimators are used (except when checking the alignment and focusing of the beam) since any collimator would produce a large neutron background.

Targets $f$ are mounted in a vertical pipe which intersects the horizontal beam pipe off-center. Through the center of the vertical pipe is placed a copper rod, at whose center four copper plates are mounted in the form of a paddle-wheel with the plates spaced 90° apart. A hole 2 in. in diameter in the center of each plate provides a place to mount a target foil. One of the four target positions is left blank so that background runs may be taken. On another one of the target positions is mounted a collimator which is used for checking the alignment and focusing of the beam. Target thicknesses were 2.65, 2.34, 2.26, and 2.44 mg/cm² for the aluminum, nickel, copper, and gold targets, respectively.

The detector assembly $(h,i,j)$ is mounted on a turntable centered directly under the beam spot. By rotating the turntable, the detector can be set accurately at any angle from 30° to 150°. A somewhat wider range of angles can be reached by mounting the detector farther from the target if the decrease in counting rate can be tolerated.

### C. Treatment of Data

The background runs are smoothed and subtracted from the corresponding target runs. After the background is subtracted, adjacent channels are grouped together to obtain points with small statistical fluctuations. The calibration data are plotted and a best power-law calibration is chosen. The derivative of this power law gives the quantity $dL/dE_p$, where $L$ is pulse height and $E_p$ is proton energy. The number of neutrons per unit area per unit energy incident on the crystal during the counting interval can be calculated by[14]

$$\frac{dN_n}{dE_{nl}}=-\frac{E_{nl}}{N_H\sigma(E_{nl})}\left[\frac{dL}{dE_p}\frac{d}{dL}\left(\frac{dL}{dE_p}\frac{dN_p}{dL}\right)\right]_{E_{nl}=E_p}, \quad (1)$$

where $E_{nl}$ is the neutron energy in the laboratory system, $N_H$ is the number of hydrogen atoms in the crystal, $\sigma$ is the total neutron-proton cross section, and $dN_p/dL$ is the number of proton pulses per unit pulse height interval after background subtraction.

An approximate correction for wall effects and second scattering in the crystal is made by dividing the spectrum above and its statistical error by[14]

$$1-0.78\frac{R_{\max}(E_{nl})}{\tau}+0.090\frac{N_H\tau}{V}\sigma(E_{nl}) +0.077\frac{N_Hr}{V}\sigma(0.068E_{nl}), \quad (2)$$

where $\tau$, $r$, and $V$ are the thickness, radius, and volume of the crystal.

A program for spectrum analysis, based on Eqs. (1) and (2), was written for use with the IBM 650 computer. The total neutron-proton cross section is computed in this program from the formulas of Hulthen and Skavlem.[16]

A further correction is made for the dead time of the analyzer by dividing the calculated neutron spectrum by the estimated value of

$$1-T_dQ^{-2}\int I^2(t)dt, \quad (3)$$

where $T_d$ is the total dead time of the analyzer, $Q$ is

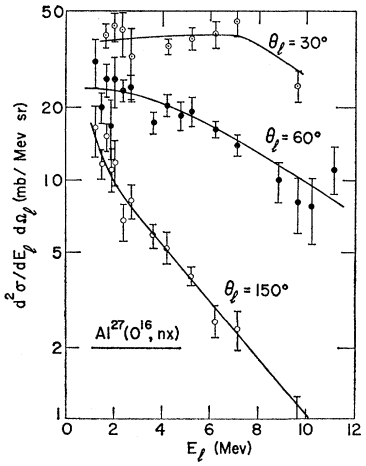


FIG. 5. Neutron energy spectra from the $Al^{27}(O^{16},nx)$ reaction in the laboratory system.

[16] L. Hulthen and S. Skavlem, Phys. Rev. 87, 297 (1952).

the charge collected during the counting interval, $t$ is time, and $I(t)$ is the instantaneous beam current.

Then the energy distribution of neutron flux (in neutrons per cm$^2$ per Mev) is converted into a double differential cross section (in the laboratory system) by using the appropriate constants

$$\frac{d^2\sigma}{dE_{nl}d\Omega_l}=\frac{M_2R^2}{DN_{\text{ion}}}\frac{dN_n}{dE_{nl}}, \tag{4}$$

where $M_2$ is the mass of a target atom, $D$ is the target density expressed as mass per unit area, $R$ is the average distance from source to detector, and $N_{\text{ion}}$ is the number of ions that pass through the target during the counting time.

### D. Center-of-Mass Transformation

To perform the transformation, center-of-mass energies and angles of emission are found as functions of laboratory energies and angles of emission, and each value of the double differential cross section in the laboratory system is multiplied by the transformation factor and plotted at its appropriate position in the c.m. system. Interpolations are usually needed to get c.m. angular distributions and energy spectra.

The derivation of the transformation factor for the double differential cross section is made by equating the integrals over corresponding regions in the two coordinate systems:

$$\int\frac{d^2\sigma}{dE_bd\Omega_b}dE_bd(\cos\theta_b)=\int\frac{d^2\sigma}{dE_ad\Omega_a}dE_ad(\cos\theta_a). \tag{5}$$

From calculus one has

$$\int\frac{d^2\sigma}{dE_bd\Omega_b}dE_bd(\cos\theta_b)=\int\frac{d^2\sigma}{dE_bd\Omega_b}\left|\frac{\partial(E_b,\cos\theta_b)}{\partial(E_a,\cos\theta_a)}\right|dE_ad(\cos\theta_a). \tag{6}$$

Since the region of integration is arbitrary and the variables of integration of the integrals on the right are the same, their integrands must be equal, i.e.,

$$\frac{d^2\sigma}{dE_ad\Omega_a}=\frac{d^2\sigma}{dE_bd\Omega_b}\left|\frac{\partial(E_b,\cos\theta_b)}{\partial(E_a,\cos\theta_a)}\right|. \tag{7}$$

Evaluating the Jacobian gives, for a Galilean transformation,

$$\frac{d^2\sigma}{dE_ad\Omega_a}=\frac{d^2\sigma}{dE_bd\Omega_b}\left(\frac{E_a}{E_b}\right)^{\frac{1}{2}}. \tag{8}$$

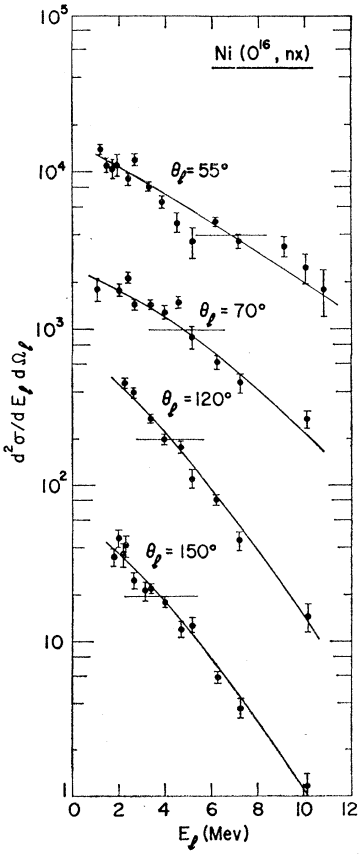


FIG. 6. Neutron energy spectra from the Ni-($O^{16}$,$nx$) reaction in the laboratory system. Each curve is intersected by a horizontal line at an absolute cross section of 20 mb Mev$^{-1}$ sr$^{-1}$.

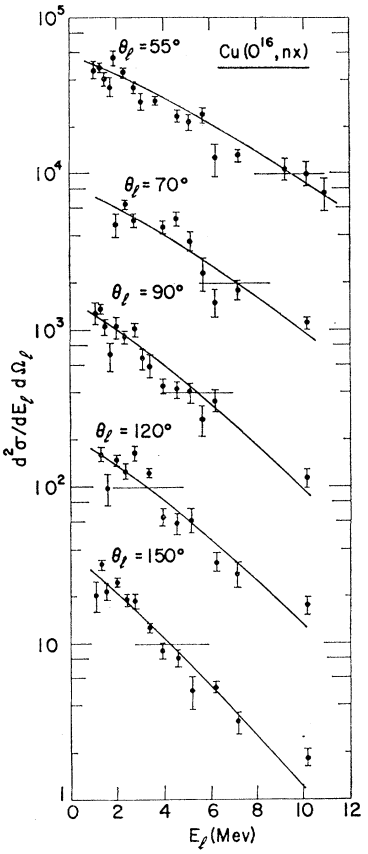


FIG. 7. Neutron energy spectra from the Cu-($O^{16}$,$nx$) reaction in the laboratory system. The horizontal lines indicate an absolute cross section of 20 mb Mev$^{-1}$ sr$^{-1}$.

A plot of the transformation factor as a function of angle and of reduced energy is shown in Fig. 4. The reduced energy is defined here as

$$E_b' \equiv E_b/\tfrac{1}{2}M_3V^2, \quad (9)$$

where $M_3$ is the mass of the observed particle and $V$ is the transformation velocity. The plot is valid for any Galilean transformation. To specialize to the case of a center-of-mass transformation, let subscripts $a$ and $b$ refer to center-of-mass and laboratory systems, respectively, and let $V$ be the velocity of the center of mass.

### E. Systematic Errors

The accuracy of the experiments is currently limited mainly by two effects: the time variation of the neutron background, and the wandering of the beam spot over the target. Both effects are believed primarily due to drift of the currents in the analyzing and focusing magnets. The background spectrum is generally at lower energy than the true spectrum. If the background varies between the time it is counted and the time that the total spectrum is counted, then the computed true spectrum may be in error, particularly at the lower energies.

Wandering of the beam spot over the target changes the distance from target to detector and the effective angle of observation and can cause errors in both the energy spectra and the angular distributions. These geometrical errors can cause errors of up to 40% in the normalization of one run to the next and even higher errors if the laboratory angular distribution varies sharply with angle.

The Faraday cup used in the experiments had an internal diameter of 3.5 in. This is adequate to catch virtually the entire beam, provided the currents in the analyzing and focusing magnets do not change drastically. As a check, the bottom of the Faraday cup was lined with paper so that the beam spot at the Faraday cup could be observed at the end of a run. Electrons were prevented from entering or leaving the Faraday cup by a magnet and by biasing the target.

Another error which is observed at very high counting rates is a slight loss of proton pulses at the smaller pulse heights as a result of occasional failure to gate the analyzer "on" when a proton pulse comes less than 10 $\mu$sec after an electron pulse. This effect limits the allowable counting rate.

## III. EXPERIMENTAL RESULTS

### A. Neutron Energy Spectra and Angular Distributions in the Laboratory System

The neutron energy spectra of the $Al^{27}(O^{16},nx)$ reaction in the laboratory system are shown in Fig. 5. The velocity of the center of mass is particularly high for this reaction and hence the laboratory angular distributions are peaked forward strongly. The spectrum of 30° is roughly constant at 40 mb Mev$^{-1}$ sr$^{-1}$ from 1.6 to 7 Mev. This spectrum does not appear to drop off until at least 7 Mev. The spectrum at 60° falls steadily with energy and the 150° spectrum falls steadily and more rapidly with energy.

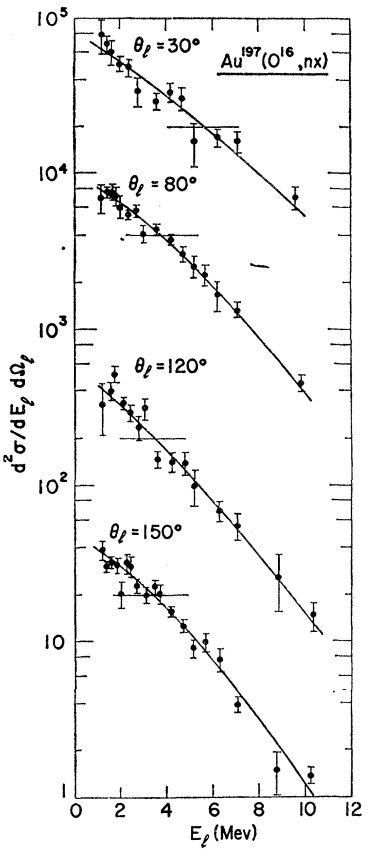


FIG. 8. Neutron energy spectra from the $Au^{197}$-$(O^{16},nx)$ reaction in the laboratory system. The horizontal lines indicate an absolute cross section of 200 mb Mev$^{-1}$ sr$^{-1}$.

The neutron energy spectra of the $Ni(O^{16},nx)$ and $Cu(O^{16},nx)$ reactions in the laboratory system are shown in Figs. 6 and 7. Horizontal lines have been drawn at an absolute cross section of 20 mb Mev$^{-1}$ sr$^{-1}$ to facilitate comparison of the curves. Center-of-mass effects are smaller than in the Al reaction, but even so the curves show an increase in absolute value at forward angles and also an increasingly rapid decline with energy as the angle increases.

The neutron energy spectra of the $Au^{197}(O^{16},nx)$ reaction in the laboratory system are shown in Fig. 8. The horizontal lines have been drawn at an absolute cross section of 200 mb Mev$^{-1}$ sr$^{-1}$. Center-of-mass effects are quite small. The spectra at different angles have nearly the same shape.

### B. Neutron Energy Spectra in the Center-of-Mass System

The neutron energy spectra of the $Al^{27}(O^{16},nx)$ reaction in the center-of-mass system are shown in Fig. 9. The large center-of-mass effect permits

measurements from 0.4 to 18 Mev in the center-of-mass system while the spectrometer is used only from 1 to 11 Mev in the laboratory. Center-of-mass angles for the 30° curve vary from 98° to 46° as energy increases over the range of points shown. Similarly the 60° curve represents c.m. angles of 124° to 80°, and the 150° curve represents c.m. angles of 165° to 158°. Since the curve at 60° lab represents c.m. angles close to 90° and since the c.m. angular distribution varies slowly in the neighborhood of 90° (as will be shown below), the curve at 60° lab can be assumed to represent an energy spectrum at 90° c.m. This method of obtaining a spectrum at constant c.m. angle avoids errors that would be produced by interpolating between runs whose normalization to one another is not exact.

The neutron energy spectra for the Ni($O^{16}$,$nx$) and Cu($O^{16}$,$nx$) reactions in the center-of-mass system are shown in Figs. 10 and 11 together with a calculation of the spectrum from the nickel reaction by Dostrovsky, *et al.*[11] The calculation was made by following the courses of 6000 evaporations by a Monte Carlo method and was normalized by assuming a collision cross section of 2.0 barns, a value obtained by interpolation from the calculations of Thomas.[17] This theoretical curve represents the cross section in mb $Mev^{-1}$ $sr^{-1}$ averaged over solid angle. At a value of 20 mb $Mev^{-1}$ $sr^{-1}$, each curve in Figs. 10 and 11 is intersected by a horizontal line to facilitate comparison. The experimental curves have nearly the same shape, but decrease with energy more rapidly than the theoretical curve. The experimental spectra at 55° lab represent c.m. angles of 94° to 65°, those at 70° lab represent c.m. angles of 110° to 81°, those at 90° lab represent

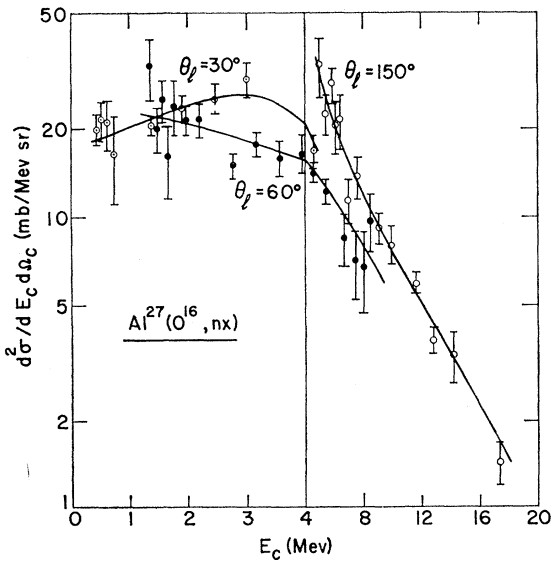


FIG. 9. Neutron energy spectra from the $Al^{27}(O^{16},nx)$ reaction in the center-of-mass system.

[17] T. D. Thomas, Phys. Rev. **116**, 703 (1959).

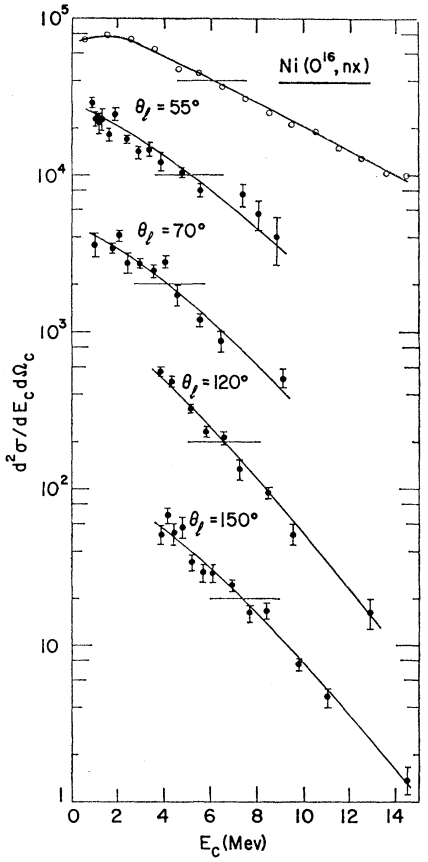


FIG. 10. Neutron energy spectra from the Ni($O^{16}$,$nx$) reaction in the center-of-mass system. The horizontal lines indicate an absolute cross section of 20 mb $Mev^{-1}$ $sr^{-1}$. The top curve was calculated for this reaction by Dostrovsky *et al.* (reference 11) and normalized by use of the cross sections calculated by Thomas (reference 17).

c.m. angles of 124° to 102°, those at 120° lab represent c.m. angles of 141° to 129°, and those at 150° lab represent c.m. angles of 161° to 155°. The energy spectra at 70° lab can be assumed to represent energy spectra at 90° c.m.

The neutron energy spectra for the $Au^{197}(O^{16},nx)$ reaction in the center-of-mass system are shown in Fig. 12. The curves are intersected by horizontal lines at 200 mb $Mev^{-1}$ $sr^{-1}$. The energy spectrum at 80° lab represents c.m. angles of 93° to 84° and hence can be assumed to represent the energy spectrum at 90° c.m.

### C. Neutron Angular Distributions in the Center-of-Mass System

From the data of Figs. 9–12, c.m. angular distributions were obtained at various c.m. energies. Angular distributions for the Al and Au reactions are shown in Figs. 13 and 14. Least-squares fits were made to a function of the form $1+B_2\cos^2\theta_c$. The fits were made under the assumption that $d^2\sigma/dE_c d\Omega_c$ can be represented as a product of a function of energy times a

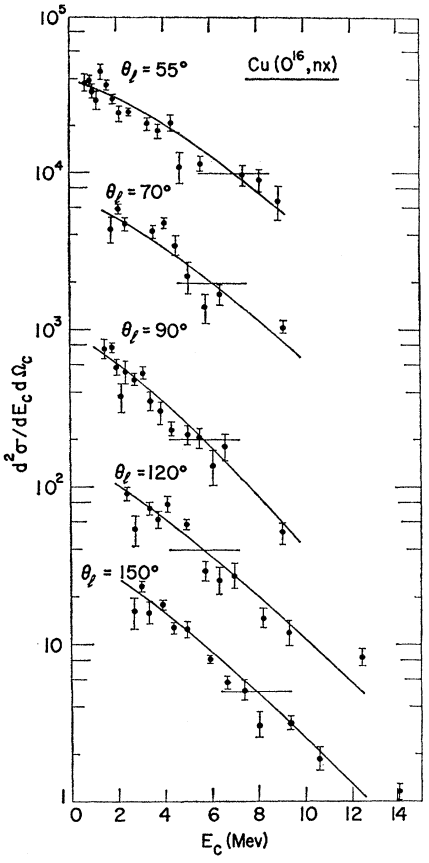


FIG. 11. Neutron spectra from the $Cu(O^{16},nx)$ reaction in the center-of-mass system. The horizontal lines indicate an absolute cross section of 20 mb $Mev^{-1}$ $sr^{-1}$.

function of angle (i.e., the assumption was made that the angular distribution is independent of neutron energy). To make the fits, the energy dependence of the 90° points on the angular distributions was represented by a simple function of energy (a power function times an exponential), the differential cross section at each data point was divided by the value of this function at the energy of the data point, and the average quotient at each angle was computed by use of statistical errors only. Then data from different angles were combined with each other and the systematic errors. Data points at energies at which data were taken at only one angle were not used. Results of this procedure must be regarded as averages over energy since theoretically the angular anisotropy should vary with the energy of the emitted particle.[18]

Results of the fit give for $B_2$ the very rough values 0.8, 2.0, 1.2, and 0.4 for the Al, Ni, Cu, and Au reactions, respectively. While statistical errors are relatively small, large systematic errors make the above numbers very untrustworthy.

In spite of the failure to obtain accurate values for $B_2$, the spectra show an obvious symmetry about 90° which indicates that the compound-nucleus evaporation theory is probably applicable. Hence the applicability of evaporation theory has been assumed in order to interpret the energy spectra. On the other hand the presence of a forward-peaking component of neutrons is not excluded, while at angles further forward than those at which the measurements were taken it is quite possible that direct or surface interactions may predominate in production of neutrons.

[18] T. Ericson, in *Advances in Physics*, edited by N. F. Mott (Taylor and Francis, Ltd., London, 1960), Vol. 9, p. 425.

### D. Total Cross Sections for Neutron Production

Total cross sections were obtained by dividing each data point by $1+B_2\cos^2\theta_c$ and plotting the quotient against $E_c$ (Figs. 15–18). The resulting spectra were integrated and multiplied by $4\pi(1+\frac{1}{3}B_2)$ to include all angles and correct roughly for the anisotropy of the angular distribution. This procedure is subject to three principal sources of error: an extrapolation is made at low energies where the differential cross section is high, any forward-peaked neutron production by direct or surface interactions is ignored, and the normalization of most of the runs may be off by as much as 40%.

Total cross sections of 2.8, 4.9, 8.1, and 25 barns were obtained for neutron production from the reactions on aluminum, nickel, copper, and gold, respectively.

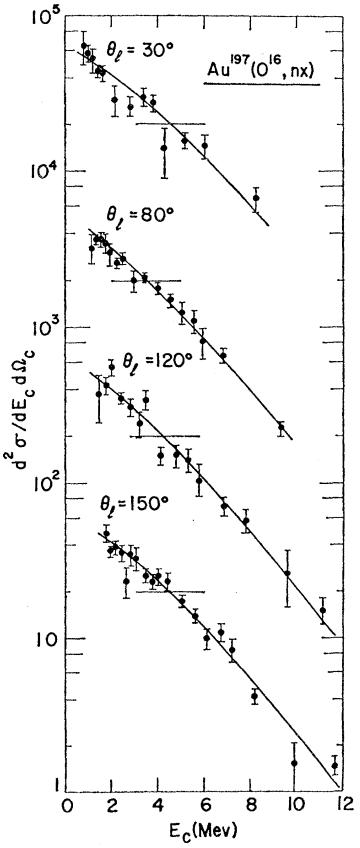


FIG. 12. Neutron energy spectra from the $Au^{197}(O^{16},nx)$ reaction in the center-of-mass system. The horizontal lines indicate an absolute cross section of 200 mb $Mev^{-1}$ $sr^{-1}$.

Each value is considerably higher than those found by Hubbard *et al.*[13] for bombardment of the same element with carbon-12 and neon-20 ions. Two possible reasons for the discrepancy are the extrapolation procedure used here, which probably overestimates the contributions from neutrons at low energies, and the escape of neutrons emitted in the forward direction from the $MnSO_4$ tank used in the experiment of Hubbard *et al.* (as those authors have pointed out).

Nevertheless both the data presented here and those of Hubbard *et al.*[13] indicate that the cross section for neutron production increases generally with the mass of the target atom (for constant beam energy and type of beam particle) but that a sharp step takes place between nickel and copper. This step is probably related to the change in average neutron excess from 2.8 for natural nickel to 5.6 for natural copper (while the atomic number changes by only one unit), and suggests that the cross sections for neutron production may be considerably different for the various isotopes of nickel and copper.

According to the Monte Carlo evaporation calculations of Dostrovsky *et al.*[11] an average of 1.87 neutrons are emitted per evaporation cascade from the reaction of oxygen on nickel. If the cross section for compound-nucleus formation is assumed to be 2.0 barns, a total neutron production cross section of 3.7 barns is thus expected. This value lies between the value of 4.9 barns found in this work and the lower values found by Hubbard *et al.*[13] for carbon-12 and neon-20 beams on nickel at 10 Mev per nucleon.

The fission cross section for the reaction of oxygen on gold has been found to be $1.8\pm0.2$ barns by Quinton *et al.*[19] who also find that the average mass of the fission fragments is 101. Most of the remaining mass (11 amu) presumably goes into neutron emission since the cross sections for proton and alpha-particle emission have been shown by Britt and Quinton[20] to be small. Thus a neutron production cross section of about 20 barns would be expected from the fission data,

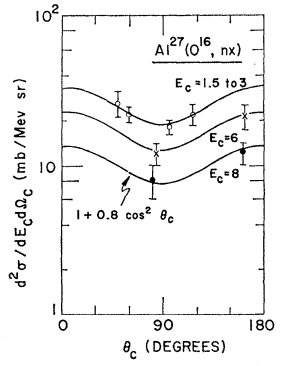


FIG. 13. Angular distributions for the $Al^{27}(O^{16},nx)$ reactions in the center-of-mass system.

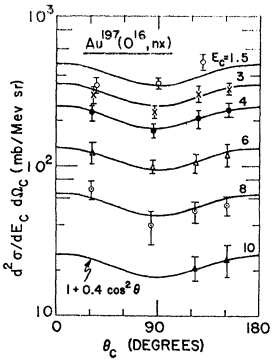


FIG. 14. Angular distributions for the $Au^{197}(O^{16},nx)$ reactions in the center-of-mass system.

if the possibility of neutron emission after fission is ignored. This value is in reasonable agreement with the 25 barns found above.

## IV. INTERPRETATION OF RESULTS

### A. Inclusion of Angular-Momentum Effects in Statistical Evaporation Theory

The nuclear evaporation formula derived by Weisskopf[1] contains a nuclear level density which includes all levels regardless of spin values. But (as Weisskopf pointed out) because of angular momentum conservation and because of the limited angular momentum that emitted light particles may take away, it is impossible to reach levels of the residual nucleus characterized by certain spin values. Such levels should not be included in the nuclear level density used in evaporation calculations. These angular momentum restrictions are very important in heavy-ion reactions at 10 Mev per nucleon, since the average orbital angular momentum of the incoming particle is about 50 $\hbar$. A compound nucleus with a spin of 50 certainly cannot reach a level of the residual nucleus with spin less than 30 by emitting a light particle, and hence most of the levels of the residual nucleus cannot be reached. It is incorrect to calculate these evaporation cascades by use of evaporation formulas that contain the level density summed over all spins.

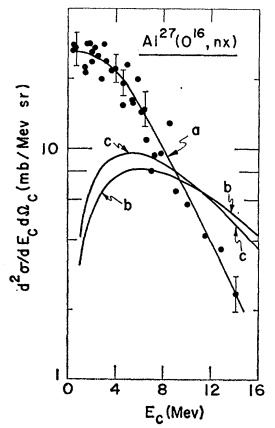


FIG. 15. Neutron energy spectra from the $Al^{27}(O^{16},nx)$ reaction in the center-of-mass system, averaged over solid angle. (a) Experimental spectrum. (b) Calculated spectrum from initial compound nucleus, charged-particle emission and angular momentum conservation being ignored. (c) Same as (b) but with effects of angular momentum included. Errors shown in Figs. 15–18 are statistical errors and do not include systematic errors.

[19] A. R. Quinton, H. C. Britt, W. J. Knox, and C. E. Anderson, Nuclear Phys. **17**, 74 (1960); H. C. Britt and A. R. Quinton, Phys. Rev. **120**, 1768 (1960).

[20] H. C. Britt and A. R. Quinton (to be published).

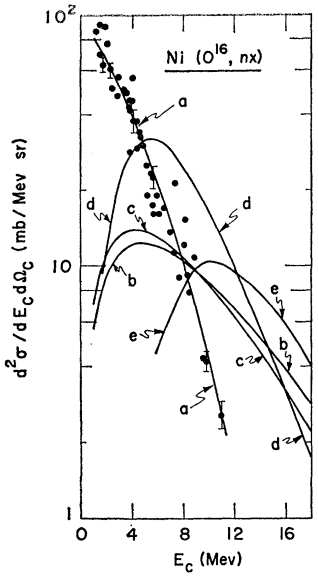


FIG. 16. Energy spectra of light particles from reactions of $O^{16}$ ions incident on Ni. (a) Experimental neutron spectrum averaged over solid angle. (b) Calculated neutron spectrum from initial compound nucleus (averaged over solid angle), charged-particle emission and conservation of angular momentum being ignored. (c) Same as (b) but with effects of angular momentum included. (d) and (e) Experimental spectra of protons and alpha particles emitted at 90° in the c.m. system, according to Knox *et al.*, (reference 10).

A new evaporation formula was derived recently by Ericson[21] under the classical approximations of spinless target, spinless projectile, spinless emitted particle, and classical addition of the outgoing orbital angular momentum and the spin of the residual nucleus. Ericson calculated the probability per unit time for a state of energy $E$ and spin $J$ to make a transition to a state of energy $E_f$ and spin $J_f$ in the final nucleus by emitting the appropriate kind of particle. He found

$$P(J,J_f,E_f)=\frac{8\pi^2 g_f}{h\rho_c(J)}\int_0^\infty \Delta^{(3)}(l,J,J_f)T_l(E_f)dl, \quad (10)$$

where $g_f$ is the statistical weight of the spin of the emitted particle, $\rho_c(J)$ is the level density of the compound nucleus, $\Delta^{(3)}$ is unity if the three vectors can form a triangle and zero otherwise, $l$ is the orbital angular momentum of the outgoing particle, and $T_l(E_f)$ is the transmission coefficient for the outgoing particle. Inserting the level density of the final nucleus $\rho_f(E_f,J_f)$, and integrating over all spins of the final nucleus gives the probability per unit time per unit energy for a nucleus of energy $E$ and spin $J$ to make a transition to a state of energy $E_f$ in the final nucleus:

$$\frac{dP}{dE_f}(J,E_f)=\frac{8\pi^2 g_f}{h\rho_c(J)}\times\int_0^\infty T_l(E_f)\left(\int_{J-l}^{J+l}\rho_f(E_f,J_f)dJ_f\right)dl. \quad (11)$$

Here the assumption has been made that $l<J$ for any value of $l$ that contributes appreciably to the integral over $l$. If the level density has negligible variation from $J-l$ to $J+l$ (curve a of Fig. 19), the integrals reduce to

$$\rho_f(E_f,J)\int_0^\infty 2lT_l(E_f)dl. \quad (12)$$

The integral here is proportional to the $\epsilon\times\sigma_{\text{reversed}}$ which appears in the Weisskopf[1] formulas. If the level density varies linearly with angular momentum (curve b of Fig. 19) the integrals still reduce to Eq. (12) even though there will be a directional correlation between $l$ and $J$. Only when the variation is nonlinear (curve c of Fig. 19) will the value of the integral be changed. For high $J$, the curve is expected to be concave upward[22] so that the average value of $\rho_f(E_f,J_f)$ will be enhanced, especially for large $l$. Particles of higher energy can be emitted with larger values of $l$ and therefore the average energy of the spectrum (from the first stage of the evaporation) is raised somewhat by this "centrifuging" effect (when $J$ is high). This "centrifuging" effect depends solely on the variation of level density with spin; another effect (temperature lowering) arises from modified energy dependences.

Equation (11) contains the level density at spins near spin $J$ instead of the level density summed over all angular momenta, $\rho_f(E_f)$, that appears in the Weisskopf[1] formula. The level density at spin $J$ can be expanded in the manner of Weisskopf to obtain

$$\rho_f(E_f,J)=\rho_f(E_{f\,\max},J)\exp[-\epsilon/T_f(E_{f\,\max},J)], \quad (13)$$

where $\epsilon$ is the energy of the emitted particle and the nuclear emission temperature $T_f$ is defined by

$$[T_f(E_{f\,\max},J)]^{-1}=\left[\frac{\partial}{\partial E_f}\ln\rho_f(E_f,J)\right]_{E_{f\,\max}} \quad (14)$$

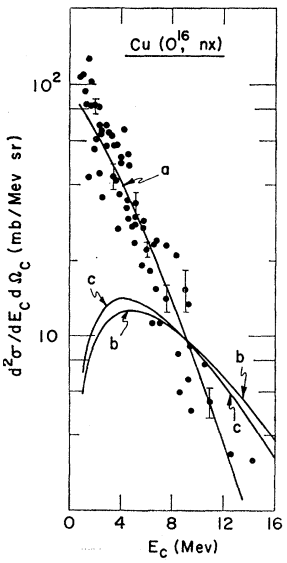


FIG. 17. Neutron energy spectra from the Cu($O^{16}$,$nx$) reaction in the center-of-mass system, averaged over solid angle. (a) Experimental spectrum. (b) Calculated spectrum from initial compound nucleus, charged-particle emission and conservation of angular momentum being ignored. (c) Same as (b) but with effects of angular momentum included.

[21] T. Ericson, Nuclear Phys. **17**, 250 (1960).

[22] T. Ericson and V. Strutinski, Nuclear Phys. **8**, 284 (1958).

instead of the usual

$$[T_f(E_{f\,\max})]^{-1}=\left[\frac{d}{dE_f}\ln\rho_f(E_f)\right]_{E_f\,\max}. \quad (15)$$

In the material below it is assumed that the variation of level density with spin is given by

$$\rho_f(E_f,J_f)=\rho_f(E_f,0)2J_f\exp(-J_f^2/2\sigma_f^2), \quad (16)$$

and that (as shown by Ericson and Strutinski[22]) the spin-cutoff parameter $\sigma_f$ is given by

$$\sigma_f^2(E_f)=\mathcal{I}T_f(E_f)/\hbar^2, \quad (17)$$

where $\mathcal{I}$ is the nuclear moment of inertia. Under the assumption that the nuclear moment of inertia varies with excitation energy much more slowly than does the nuclear temperature, the relation between nuclear temperatures can be shown to be

$$[T_f(E_f,J_f)]^{-1}=[T_f(E_f)]^{-1}+\left(\frac{J_f^2}{2\sigma_f^2}-1\right)\frac{d}{dE_f}\ln T_f(E_f). \quad (18)$$

For the reactions studied, Thomas'[17] calculated value for the average orbital angular momentum of the incoming particle is greater than $\sqrt{2}\sigma_f$ calculated by Eq. (17) and so

$$T_f(E_f,J)<T_f(E_f) \quad (19)$$

for the first stage of the evaporation when $J$ is large. This temperature-lowering effect tends to reduce the average energy of the spectrum and counteract the "centrifuging" effect. A detailed calculation is necessary to see which effect dominates.

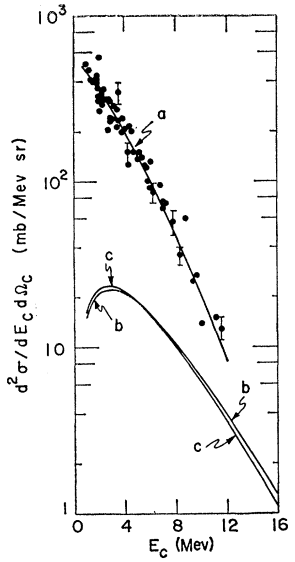


FIG. 18. Neutron energy spectra from the $Au^{197}(O^{16},nx)$ reaction in the center-of-mass system, averaged over solid angle. (a) Experimental spectrum. (b) Calculated spectrum from initial compound nucleus, charged-particle emission and conservation of angular momentum being ignored. (c) Same as (b) but with effects of angular momentum included.

## B. Calculation of the Effects of Angular-Momentum Restrictions upon Neutron Energy Spectra

Calculations of the neutron spectra emitted from fully excited compound nuclei were performed for the four reactions studied experimentally. The calculations do not include neutrons from lower points on the evaporation cascade. Equation (11) was divided by the total probability for evaporating any particle, then multiplied by the cross section for formation of a compound nucleus with spin $J$. The product was integrated over $J$ to get the cross section per unit energy for emission of a particle of type $f$,

$$\frac{d\sigma}{d\epsilon_f}=2\pi\lambda\!\!\!^{-}_i{}^2\int_0^\infty dJ\,T_J^{(i)}J\frac{g_f\rho_f(E_f,J)\sigma_f^2\int_0^\infty dl\,T_l\exp(-l^2/2\sigma_f^2)\sinh(Jl/\sigma_f^2)}{\sum_f g_f\int_0^{E_f\,\max}dE_f\,\rho_f(E_f,J)\sigma_f^2\int_0^\infty dl\,T_l\exp(-l^2/2\sigma_f^2)\sinh(Jl/\sigma_f^2)}, \quad (20)$$

where the integration over $J_f$ was done with the aid of Eq. (16). Equation (20) may also be obtained from a formula of Ericson [Eq. (5.26) of reference 18] by a simple integration over directions of the outgoing particle and a few algebraic steps. In Eq. (20), $\lambda\!\!\!^{-}_i$ is the deBroglie wavelength of the incoming particle, $J$ is both its orbital angular momentum and the spin of the compound state, and $T_J^{(i)}$ is the transmission coefficient for the incoming particle.

The calculation, made under the assumption that only neutrons are emitted, was done in the sharp-cutoff approximation under which Eq. (20) reduces to[23]

$$\frac{d\sigma}{4\pi d\epsilon}=\frac{\lambda\!\!\!^{-}_i{}^2}{2}\int_0^{J_{\max}}dJ\,J\frac{\exp[-\epsilon/T_f(E_{f\,\max},J)]\int_0^{K\epsilon^{\frac{1}{2}}}dl\exp(-l^2/2\sigma_f^2)\sinh(Jl/\sigma_f^2)}{\int_0^\infty d\epsilon\exp[-\epsilon/T_f(E_{f\,\max},J)]\int_0^{K\epsilon^{\frac{1}{2}}}dl\exp(-l^2/2\sigma_f^2)\sinh(Jl/\sigma_f^2)}, \quad (21)$$

[23] Similar formulas based on the same classical approximations have been used by T. Kammuri and R. Nakasima in *Reactions Between Complex Nuclei*, edited by A. Zucker, F. T. Howard, and E. C. Halbert (John Wiley & Sons, Inc., New York, 1960), p. 301, and by H. W. Broek, thesis, Yale University, 1960 (unpublished).

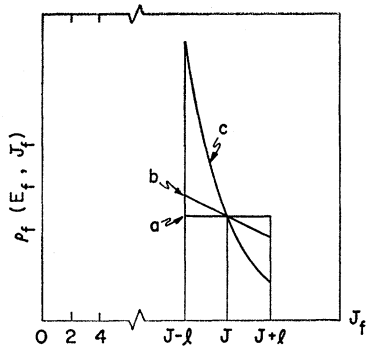


FIG. 19. Variation of level density with spin. (a) No dependence of level density upon spin for the possible values of $J_f$. (b) Linear dependence. Correlation in direction between $l$ and $J$, but same average value of ordinate as for case (a). (c) Nonlinear dependence. Strong correlation in direction between $l$ and $J$. Enhanced average value of ordinate, especially for high values of $l$.

where

$$J_{\max}^2 \equiv \sigma_c/\pi\lambda\!\!\!^{-}_i{}^2, \tag{22}$$

$\sigma_c$ is the collision cross section calculated by Thomas,[17] $\epsilon$ is the energy of the emitted neutron, and

$$K = r_0 A^{\frac{1}{3}} \hbar^{-1} (2M_3)^{\frac{1}{2}}, \tag{23}$$

where $r_0 A^{\frac{1}{3}}$ is the radius of the residual nucleus and $M_3$ is the mass of the neutron. The radius parameter $r_0$ was taken to be 1.5 f.

Table I shows the quantities of interest, beginning with the kinetic energy available in the c.m. system and the maximum excitation energy after emission of one neutron. Next are presented the collision cross section $\sigma_c$ and average orbital angular momentum $\bar{L}$, of the incoming particle, both calculated by Thomas.[17] (The values for nickel were obtained by interpolation.) However, it is not certain whether collisions involving the highest possible angular momenta produce compound nuclei or not. These collisions may lead to fragmentation or grazing processes such as those observed by Anderson *et al.*[24] and by Kaufmann and Wolfgang[25] rather than to evaporation reactions. Thus the average orbital angular momentum of collisions producing compound nuclei may be less than the $\bar{L}$ used in these computations.

The quantity $\bar{L}/A$ is a measure of the extent to which the motions of the nucleons are ordered into rotation about an axis. This quantity increases with decreasing atomic mass, and so angular momentum effects may be more important for targets of low atomic number even though the total angular momentum is less.

The nuclear thermodynamic temperature $t$ was calculated from Cameron's[26] expressions. The nuclear emission temperature[27] was then found by

$$[T(E)]^{-1} = [t(E)]^{-1} - (5/4E). \tag{24}$$

The nuclear emission temperature at spin $J=\bar{L}$ was found by use of Eq. (18). The spin-cutoff parameter was found from Eq. (17) with a rigid-body moment of inertia and a nuclear-radius parameter $r_0 = 1.5$ f.

The results of the computations, done on an IBM-704 computer, are shown as curves b and c of Figs. 15–18. Curves b represent calculated neutron spectra from the initial compound nuclei, charged-particle emission and conservation of angular momentum being ignored. Curves c include the angular-momentum effects discussed above. None of the curves include neutrons from later stages of the evaporation cascades. The results of the computations show that temperature lowering is the dominant angular-momentum effect on the neutron spectra from fully excited compound nuclei for the parameters chosen.

The computations were repeated with $\sigma_c$ reduced by a factor of 2 so that, by Eq. (22), $J_{\max}$ was reduced by a factor of $2^{\frac{1}{2}}$. The results show that, for the cases studied, this reduction in $\sigma_c$ reduces the angular momentum effects upon the spectra. The computations were also repeated with the values of $K$ computed from different values of the radius parameter. The results show that increasing $K$ decreases the average energy of the spectra slightly for the cases studied. Computations in which the spin-cutoff parameter was arbitrarily changed indicate that if the nuclear moment of inertia is less than the rigid-body value used in the original computations then the angular-momentum effects upon the spectra may be more important than the effects shown in Figs. 15–18.

### C. Comparison of Energy Spectra

In comparing the measured neutron energy spectra with the calculations, four facts must be kept in mind: (a) The calculations are only for the first particle emitted in evaporation cascades. (b) The calculations assumed that only neutrons are emitted as the first

TABLE I. Quantities of interest in compound-nucleus reactions induced by 160-Mev oxygen-16 ions.

| Target | $Al^{27}$ | Ni | Cu | $Au^{197}$ |
|---|---|---|---|---|
| $E_{c.m.}$ (Mev) | 100 | 126 | 128 | 148 |
| $E_{f\,\max}$ (Mev) | 101 | 108 | 116 | 110 |
| $\sigma_c$ (barns) | 1.71 | 2.0 | 2.04 | 2.20 |
| $\bar{L}$ | 34.4 | 46 | 48.2 | 59.3 |
| $\bar{L}/A$ | 0.80 | 0.62 | 0.61 | 0.28 |
| $t$ (Mev) | 5.67 | 4.50 | 4.51 | 3.12 |
| $T_f(E_{f\,\max})$ (Mev) | 6.10 | 4.76 | 4.72 | 3.22 |
| $T_f(E_{f\,\max}, \bar{L})$ (Mev) | 4.92 | 4.11 | 4.12 | 3.11 |
| $\sigma_f$ | 8.14 | 11.4 | 12.0 | 32.2 |

[24] C. E. Anderson, W. J. Knox, A. R. Quinton, and G. R. Bach, Phys. Rev. Letters **3**, 557 (1959).
[25] R. Kaufmann and R. Wolfgang, Phys. Rev. **121**, 192 and 206 (1961).
[26] A. G. W. Cameron, Can. J. Phys. **36**, 1040 (1958).
[27] The distinction between the nuclear thermodynamic temperature and the nuclear emission temperature is discussed by J. M. B. Lang and K. J. LeCouteur, Proc. Phys. Soc. (London) **A67**, 586 (1954).

particle in the evaporation cascades. (c) The cross sections for formation of compound nuclei may be less than the cross sections calculated by Thomas[17] because of grazing reactions.[24,25] (d) The nuclear temperatures used in the computations may be too high.[28]

Particles emitted late in the evaporation cascades are emitted from nuclei of lower temperature so that at the lower energies the experimental spectra should be much larger than the calculated ones. This effect is seen for all four reactions (Figs. 15–18).

The high-energy end of the experimental energy spectra should be due mostly to neutrons emitted near the beginning of the evaporation cascades. Emission of some of the neutrons from partly de-excited nuclei should make the slopes of the high-energy ends of the experimental curves be slightly more negative than those of the corresponding theoretical curves. This effect, which is seen for all four reactions, makes it difficult to judge whether or not the nuclear temperature has been chosen correctly. The evaporation calculation must be extended to the entire cascade to make a good comparison possible. The only evaporation calculation carried through the entire cascade is that of Dostrovsky *et al.*[11] for the nickel reaction. Their spectrum is shown in Fig. 10. Their calculation, which does not include the angular-momentum effects, gives a spectrum which is quite close to the experimental spectra but which decreases with energy somewhat less rapidly than the experimental ones.

[28] D. B. Beard, Phys. Rev. Letters 3, 432 (1959).

The experimental spectra are lower than the calculated ones at the upper end of the spectrum for the aluminum, nickel, and copper reactions. The most likely explanation is that charged-particle emission presumably competes with neutron emission at the start of the cascade. For the Ni reaction, emission of protons and alpha particles from compound nuclei has been studied by Knox *et al.*[10] Their spectra at 90° c.m. (curves d and e in Fig. 16) show that charged-particle emission has quite a large cross section. Other explanations for the discrepancy between the high-energy ends of the experimental and theoretical spectra are that the cross sections for compound-nucleus formation may be less than the values used or that too high a temperature may have been used in the calculations.

For the Au reaction, the emission cross sections for protons and alpha particles are 0.46 and 0.76 barn, respectively, according to Britt and Quinton,[20] and not all of each cross section is due to emission from a compound nucleus. Hence evaporation of charged particles is much less probable than that of neutrons. Thus the experimental and calculated curves in Fig. 18 should be expected to meet at their upper ends. Data at higher energies are needed to test this expectation although the present data are consistent with it.

## ACKNOWLEDGMENTS

The author is very grateful to Dr. Carl E. Anderson and Dr. William J. Knox for their guidance and encouragement during this project. The author would like to express his thanks to Dr. D. Allen Bromley and Dr. John R. Huizenga for valuable discussions.